Cooling a mechanical resonator to the quantum regime by heating it

Yue Ma,[1,2] Zhang-qi Yin,[1,*] Pu Huang,[3] W. L. Yang,[4] and Jiangfeng Du[3,†]

[1]*Center for Quantum Information, Institute for Interdisciplinary Information Sciences, Tsinghua University, Beijing 100084, China*

[2]*Department of Physics, Tsinghua University, Beijing 100084, China*

[3]*Hefei National Laboratory for Physics Sciences at Microscale and Department of Modern Physics, University of Science and Technology of China, Hefei 230026, China*

[4]*State Key Laboratory of Magnetic Resonance and Atomic and Molecular Physics, Wuhan Institute of Physics and Mathematics, Chinese Academy of Sciences, Wuhan 430071, China*

(Received 18 April 2016; published 18 November 2016)

We consider a mechanical resonator made of diamond, which contains a nitrogen-vacancy center (NV center) locating at the end of the oscillator. A second-order magnetic gradient is applied and induces coupling between mechanical modes and the NV center. By applying a proper external magnetic field, the energy difference between NV center electron spin levels can be tuned to match the energy difference between two mechanical modes a and b. A laser is used for continuously initializing the NV center electron spin. The mode a with lower frequency is driven by a thermal bath. We find that the temperature of the mode b is significantly cooled when the heating bath temperature is increased. We discuss the conditions that quantum regime cooling requires and confirm the results by numerical simulation. Finally we give the intuitive physical explanation of this unusual effect.

DOI: 10.1103/PhysRevA.94.053836

I. INTRODUCTION

Cooling and manipulating the motion of a mechanical resonator are widely studied [1]. They have many applications in quantum information science [2–9], testing quantum effects in macroscopic systems [10–20], ultrasensitive sensing [21–26], etc. In order to a cool mechanical resonator, we should couple it to other cold systems such as cavity mode (optomechanics) [27–29], electronic spin (nitrogen-vacancy [NV] centers) [30–32], etc. In optomechanics, laser cooling of mechanical resonators is a typical method. Intuitively, this is not hard to understand. A laser produces coherent light, which is well ordered (cold), and will make the mechanical system couple with a colder cavity bath [27,28]. However, counterintuitively, recent research showed that a thermal light, which is very hot, can also cool an optomechanical system [33]. In this system, the mechanical resonator to be cooled is coupled with two optical modes [34]. The low-frequency mode is in contact with a hot thermal light while the high-frequency mode is not, acting as an auxiliary part. After the system reaches the equilibrium state, the thermal phonon number in the mechanical mode will be smaller.

In a hybrid system that contains a NV center and a mechanical resonator, a magnetic gradient is applied to couple the NV center with the resonator. The NV center is continuously initialized by a laser and could be used for cooling the mechanical resonator to the ground state [30]. In previous literatures, the first-order magnetic gradient was used for inducing coupling between the NV center and the mechanical mode [30,35–40]. It is quite natural to ask whether the higher order magnetic gradient could be useful for coupling the NV center and the mechanical resonator and cooling it.

In this paper, we consider a system that contains a mechanical cantilever and a NV center [40]. A second-order magnetic gradient is applied to induce the coupling between the NV center and the two mechanical modes a and b. The electron spin transition frequency of the NV center is tuned to match the mechanical modes' frequency difference. The NV center is continuously reset to the ground state by a laser. In this way, the NV center acts as an effective vacuum bath to cool the mode b. An incoherent driving (thermal bath) is applied on the lower frequency mode a, which results in a higher temperature. The incoherent driving on mode a also increases the effective coupling between mode b and the NV center, and cools the mode b. We find that the quantum regime cooling is possible under the current experimental conditions.

The paper is organized as follows. In Sec. II, we introduce the scheme of the second-order magnetic field gradient induced coupling between an NV center and mechanical modes. In Sec. III, we derived the analytical solution for the system. In Sec. IV, the analytical results are verified by numerical simulation. In Sec. V, discussion and conclusion are given.

II. THE SCHEME

As shown in Fig. 1, we consider a diamond cantilever resonator that contains a NV center at the end of it. Two mechanical modes a and b are under consideration, with frequencies $\omega_a < \omega_b$. Two spin states of the NV center electron are relevant here, $|-1\rangle$ and $|0\rangle$. By applying a proper magnetic field, the energy split between the two states of the NV center, ω_z, is equal to the energy difference of the two mechanical modes, $\Delta = \omega_b - \omega_a$. Due to the second-order magnetic gradient $G_2 = \partial^2 B/\partial x^2$, the two mechanical modes a and b both couple with the NV center.

Initially, both mechanical modes a and b are in the thermal states with the average thermal phonon number $\bar{n}_a$ and $\bar{n}_b$. The mode a is driven by a thermal bath with average phonon number much higher than its environment. The NV center electron spin is initialized to the $|0\rangle$ state at the beginning. The Hamiltonian of the whole system can be expressed as $H = H_0 + H_1$, where H_0 is the noninteraction part and H_1

*yinzhangqi@mail.tsinghua.edu.cn

†djf@ustc.edu.cn

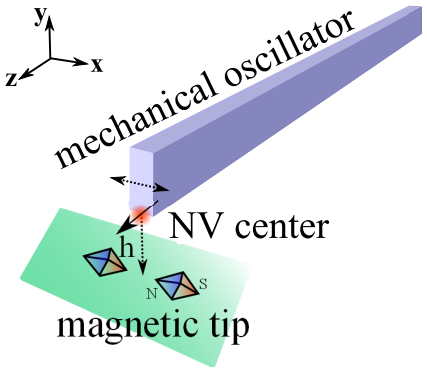

FIG. 1. A nanodiamond is fabricated as a thin cantilever which can oscillate along the x axis, while the defect of an NV center is at the end. Two magnetic tips, which point along the x axis and generate second-order magnetic gradient along the x axis, are placed below the cantilever. The distance between the midpoint of the connection lines of the tips and the NV center are around 50 nm. An external static magnetic field $B_{\rm ext}$ is added along the z axis to induce Zeeman split in order to drive away the NV center spin $|+1\rangle$ state and keep the $|0\rangle$ and $|-1\rangle$ state closer.

describes the interaction between the mechanical resonator and the NV center electron spin:

$$\begin{aligned} H_0 &= \frac{\omega_z}{2}\sigma_z + \omega_a a^\dagger a + \omega_b b^\dagger b, \\ H_1 &= [g_a a^\dagger a + g_b b^\dagger b + g_{ab}(a^\dagger b + a b^\dagger)]\sigma_x, \end{aligned} \tag{1}$$

where $g_a = g_s\mu_B G_2 x_a^2$, $g_b = g_s\mu_B G_2 x_b^2$, and $g_{ab} = g_s\mu_B G_2 x_a x_b$; $x_a = \sqrt{\hbar/2m_a\omega_a}$ ($x_b = \sqrt{\hbar/2m_b\omega_b}$) is the zero-field fluctuation for the mechanical mode a (b); and m_a (m_b) is the effective mass for mode a (b). Experimentally, $\omega_z \sim 2\pi \times 10^7$ Hz, and $g_a, g_b, g_{ab} \sim 2\pi \times 1$ Hz can be realized (see Appendix A).

Under the rotating wave approximation, which shifts the energy zero point by $\omega_a(a^\dagger a + b^\dagger b)$, we can change H_0 into

$$H_0' = \frac{\omega_z}{2}\sigma_z + \Delta b^\dagger b. \tag{2}$$

Unavoidably, the system will go through some intrinsic loss. The mechanical decays γ_a and γ_b are of the order of $2\pi \times 1$ Hz (see Appendix A). The intrinsic decay rate Γ_0 for NV center is much less than 1 Hz at low temperature. By adding an initializing laser, the decay rate Γ for the NV center electron spin would be much larger than the decay rates for the mechanical modes γ_a and γ_b. The dephasing of NV center is neglected, as it could be eliminated by continuous dynamical decoupling [41]. However, as we will use the same model to describe the decay of the spin and the vibration, here we should make sure that $\Gamma, \gamma_a, \gamma_b \ll \omega_z$. As the evolution of the system contains decay and damping, it is convenient to describe it with a quantum master equation [42], which can be written out explicitly as

$$\begin{aligned} \dot\rho &= -i[H,\rho] + (\mathcal{L}_a + \mathcal{L}_b + \mathcal{L}_s)\rho, \\ \mathcal{L}_a &= (1+\bar n_a)\gamma_a D_a + \bar n_a \gamma_a D_{a^\dagger}, \\ \mathcal{L}_b &= (1+\bar n_b)\gamma_b D_b + \bar n_b \gamma_b D_{b^\dagger}, \\ \mathcal{L}_s &= \Gamma D_{\sigma_-}. \end{aligned} \tag{3}$$

D_x refers to the notation in Lindblad form, which is $D_x(\rho) = 2x\rho x^\dagger - x^\dagger x\rho - \rho x^\dagger x$. Equation (3) will be solved in both analytical and numerical methods. The results of the both methods will be compared and discussed.

III. ANALYTICAL SOLUTION

As mentioned above, the phonon bath for mode a is very large, so the average phonon number of mode a is almost always equal to the average phonon number in the bath, that is, $\langle a^\dagger a\rangle = \bar n_a$. Moreover, as the phonon number of mode b is much smaller than that of mode a, it is safe to drop the term $b^\dagger b$ in H_1. If we denote $\delta = a^\dagger a - \bar n_a$ as the phonon occupation number fluctuation of mode a, under the rotating wave picture, H_1 can be simplified to

$$H_1' = g_a\delta(\sigma_+ + \sigma_-) + g_{ab}(a^\dagger b\sigma_+ + a b^\dagger \sigma_-). \tag{4}$$

For the convenience of the notation, here we rename $H_0' \to H_0$, $H_1' \to H_1$.

Using the standard method of quantum master equation [43], and after adiabatically eliminating the mode a [44,45], we can get the reduced master equation for mode b and the electron spin mode s (see Appendix B)

$$\begin{aligned} \dot\rho_{b,s}(t) &= -i[H_0, \rho_{b,s}(t)] + \mathcal{L}_b\rho_{b,s}(t) + \mathcal{L}_s\rho_{b,s}(t) \\ &\quad + \mathcal{L}_1\rho_{b,s}(t) + \mathcal{L}_2\rho_{b,s}(t), \end{aligned} \tag{5}$$

where we have introduced two Liouvillians for convenience:

$$\begin{aligned} \mathcal{L}_1 &= \frac{g_{ab}^2}{\gamma_a+\gamma_b+\Gamma}[(1+\bar n_a)D_{b\sigma_+} + \bar n_a D_{b^\dagger\sigma_-}] \\ \mathcal{L}_2 &= \frac{(2\gamma_a+\Gamma)g_a^2(\bar n_a^2+\bar n_a)}{\omega_z^2 + (2\gamma_a+\Gamma)^2}(D_{\sigma_+} + D_{\sigma_-}). \end{aligned} \tag{6}$$

Equation (6) can be written in a more compact form if we define the effective average excitation number of the NV center electron spin as

$$n_s' = \frac{(2\gamma_a+\Gamma)g_a^2(\bar n_a^2+\bar n_a)}{\Gamma[\omega_z^2 + (2\gamma_a+\Gamma)^2]}. \tag{7}$$

In fact, n_s' is very close to zero because of the weak coupling requirement ($g_a\sqrt{\bar n_a}, g_b\sqrt{\bar n_b}, g_{ab}\sqrt{\bar n_a \bar n_b} \ll \omega_z$), in other words, due to the large energy split ω_z and the relative large damping rate Γ. Then we can define an effective Liouvillian for the spin as well $\mathcal{L}_s' = \mathcal{L}_s + \mathcal{L}_2 = (1+n_s')\Gamma D_{\sigma_-} + n_s'\Gamma D_{\sigma_+}$.

Now the equation of motion for the reduced density matrix $\rho_{b,s}$ becomes

$$\dot\rho_{b,s}(t) = -i[H_0, \rho_{b,s}(t)] + \mathcal{L}_1\rho_{b,s}(t) + \mathcal{L}_b\rho_{b,s}(t) + \mathcal{L}_s'\rho_{b,s}(t). \tag{8}$$

The corresponding adjoint equations for the phonon number operator $\hat n_b = b^\dagger b$ and excitation number operator $\hat n_s = \sigma_+\sigma_-$ can be developed then (see Appendix C);

$$\begin{aligned} \frac{d}{dt}\hat n_s &= \frac{2g_{ab}^2}{\gamma_a+\gamma_b+\Gamma}[(-2\bar n_a - 1)\hat n_b\hat n_s - \bar n_a\hat n_s + (\bar n_a+1)\hat n_b] \\ &\quad + 2\Gamma[(-2n_s'-1)\hat n_s + n_s'], \\ \frac{d}{dt}\hat n_b &= \frac{2g_{ab}^2}{\gamma_a+\gamma_b+\Gamma}[(2\bar n_a+1)\hat n_b\hat n_s + \bar n_a\hat n_s - (\bar n_a+1)\hat n_b] \\ &\quad + 2\gamma_b(\bar n_b - \hat n_b). \end{aligned} \tag{9}$$

Taking the average on both sides with respect to the quantum state of the system, and under average field approximation which refers to $\langle \hat{n}_b \hat{n}_s \rangle = \langle \hat{n}_b \rangle \langle \hat{n}_s \rangle$, the stationary state for the average phonon number of mode b can be solved from the quadratic equation below after we drop the nonphysical solution:

$$A\langle \hat{n}_b \rangle^2 + B\langle \hat{n}_b \rangle + C = 0, \tag{10}$$

where

$$\begin{aligned} A &= \frac{-\gamma_b g_{ab}^2 (2\bar{n}_a + 1)}{\gamma_a + \gamma_b + \Gamma}, \\ B &= \frac{g_{ab}^2}{\gamma_a + \gamma_b + \Gamma}(2\bar{n}_a\bar{n}_b\gamma_b + \bar{n}_b\gamma_b - \bar{n}_a\gamma_b \\ &\quad - \Gamma\bar{n}_a - \Gamma n_s^{'} - \Gamma) - \gamma_b\Gamma(2n_s' + 1), \\ C &= \frac{g_{ab}^2}{\gamma_a + \gamma_b + \Gamma}\bar{n}_a(\gamma_b\bar{n}_b + \Gamma n_s') + \gamma_b\bar{n}_b\Gamma(2n_s' + 1). \end{aligned} \tag{11}$$

In Fig. 2, the stationary phonon number of mode b is plotted as a function of the average phonon number of mode a. Unlike the previous Ref. [33], where there was an optimal heating bath temperature, here increasing the heating bath temperature will always cool the resonator, which is an outstanding property. As environmental temperature increases, the quantum regime cooling $\langle \hat{n}_b \rangle < 1$ can be realized by increasing both the mode a temperature and NV center decay Γ.

We can further look at how different values of Γ can change the effect of cooling. The qualitative trend can be seen clearly from Fig. 3. For a given value of $\bar{n}_a$, when Γ increases from a small value to a relative large value, there exists a certain Γ for

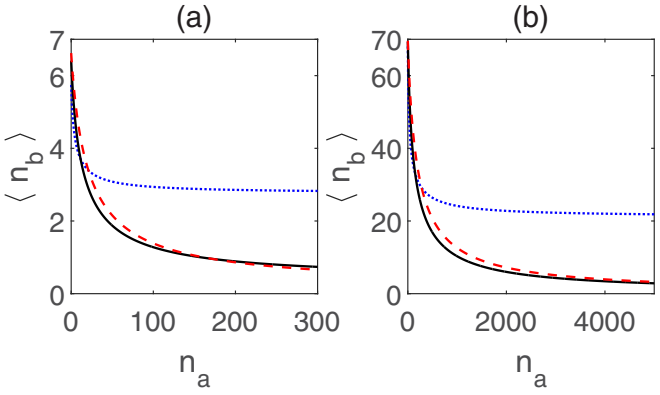

FIG. 2. $\langle \hat{n}_b \rangle$ as a function of $\bar{n}_a$. The parameters related to frequency are $\omega_z/2\pi = 2 \times 10^7$ Hz, $g_a/2\pi = 3$ Hz, $g_b/2\pi = 1$ Hz, $g_{ab}/2\pi = \sqrt{3}$ Hz, and $\gamma_a/2\pi = \gamma_b/2\pi = 1$ Hz. (a) The initial temperature of mode b is 10.8 mK. The average phonon number is approximated by the Bose distribution $\bar{n}_b = 1/(e^{\frac{\hbar\omega_b}{k_B T}} - 1) = 7$. Three values of $\Gamma/2\pi = 10,30,50$ Hz correspond to the blue dotted line, black solid line, and red dashed line, respectively. $\Gamma/2\pi = 30$ Hz and 50 Hz can reach ground-state cooling ($\langle \hat{n}_b \rangle < 1$) if $\bar{n}_a > 160$. This corresponds to an effective temperature $T_a = 77.1$ mK. (b) The initial temperature of mode b is $T = 101.4$ mK. The thermal phonon number is $\bar{n}_b = 70$. The blue dotted, black solid, and red dashed lines correspond to $\Gamma/2\pi = 100,300,500$ Hz, respectively. Ground-state cooling can be reached if $\Gamma/2\pi = 300$ Hz and $\bar{n}_a > 22\,500$ ($T_a = 10.8$ K), or $\Gamma/2\pi = 500$ Hz and $\bar{n}_a > 19\,700$ ($T_a = 9.5$ K).

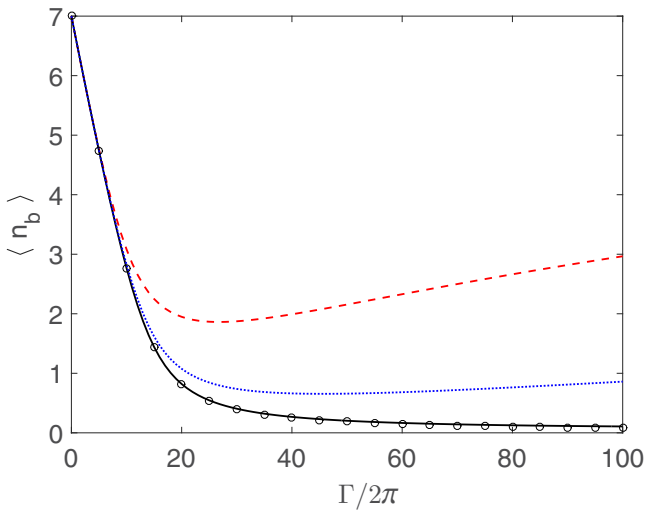

FIG. 3. $\langle \hat{n}_b \rangle$ as a function of $\Gamma/2\pi$. Three values of $\bar{n}_a$, 50, 300, and 10 000, correspond to the red dashed line, the blue dotted line, and the black solid line. Black circles display Eq. (13) in the limit of $\bar{n}_a \to \infty$. The initial temperature of mode b is 10.8 mK so $\bar{n}_b = 7$. Other parameters are the same as in Fig. 2.

which the cooling effect is the largest. Before the optimal cooling point, Γ is not large compared with the effective coupling (e.g., $g_a\sqrt{\bar{n}_a}$), so increased Γ will benefit the cooling process. However, after that, larger Γ will result in a smaller cooling rate. When $\bar{n}_a$ increases, the optimal Γ will increase, too. In the limit of $\bar{n}_a \to \infty$, we can get a simple expression for $\langle \hat{n}_b \rangle$ under the weak coupling assumption

$$\langle \hat{n}_b \rangle = \frac{1}{2}\left[\bar{n}_b - \frac{\gamma_b + \Gamma}{2\gamma_b} + \sqrt{\left(\bar{n}_b - \frac{\gamma_b + \Gamma}{2\gamma_b}\right)^2 + 2\bar{n}_b}\right]. \tag{12}$$

As shown in Fig. 3, such an approximation is quite reasonable. In the limit of $\bar{n}_a \to \infty$, the condition for quantum regime cooling ($\langle \hat{n}_b \rangle < 1$) is

$$\Gamma > 3\gamma_b(\bar{n}_b - 1), \tag{13}$$

which can be fulfilled by tuning Γ with laser. These analytical results are based on the rotating wave approximation (RWA). When thermal phonon number $\sqrt{\bar{n}_a} \sim \Delta/g_{ab}$, the RWA is no longer valid. From the parameters used in Fig. 2, RWA requires $\bar{n}_{ab} < 10^{12}$, which is obviously fulfilled in Fig. 2 and the following figures in this paper.

IV. NUMERICAL SIMULATION

Now we discuss the numerical simulation of the cooling process, and compare the result with the analytical ones above. The idea is simple. We expand the quantum operators and quantum states in the uncoupled representation, that is, the Kronecker tensor product of the occupation number representations for the three modes involved. The matrix forms of Eq. (3) can then be calculated step by step with the classical four-order Runge-Kutta method. The average phonon number for mode b is equal to $\mathrm{tr}(\rho N_b)$, where N_b is the phonon number operator of mode b in the whole Hilbert space for the

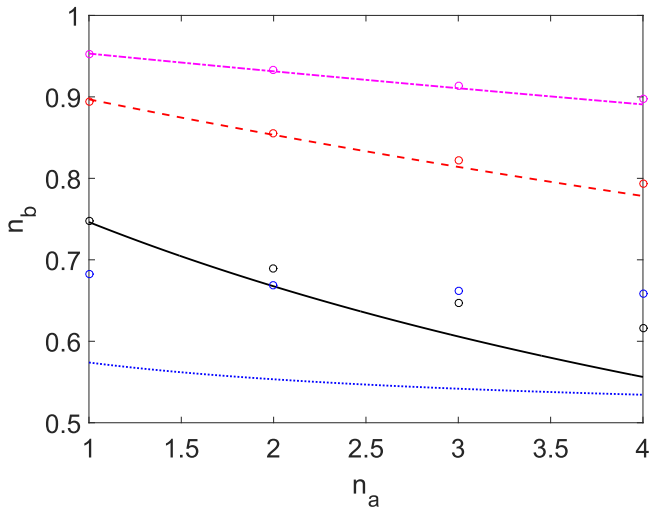

FIG. 4. Comparison of analytical and numerical results. Lines (circles) represent analytical (numerical) results. We choose four $\Gamma/2\pi$: 2, 15, 50, and 120 Hz, corresponding to the blue dotted line (blue circles), black solid line (black circles), red dashed line (red circles), and pink dash-dotted line (pink circles). The initial phonon number for mode b is taken as $\bar{n}_b = 1$. Other parameters are the same as in Fig. 2.

system, namely, $N_b = I_s \otimes I_a \otimes (b^\dagger b)$. It should be pointed out, however, as the dimension of a matrix cannot be too large for a numerical simulation, the requirement $\bar{n}_a \gg \bar{n}_b$ is not able to be satisfied here. As a result, H_1 in Eq. (1) should be inserted in the equation of motion Eq. (3) instead of H_1'.

We present several numerical results of the stationary phonon number $\langle \hat{n}_b \rangle$ with the results we get from Eq. (10), which is plotted in Fig. 4. As can be seen from the figure, when $\Gamma \gg \gamma_a, \gamma_b$ is satisfied, the analytical results match the numerical ones perfectly. But when γ_a and γ_b are comparable with Γ, the two results no longer agree with each other quantitatively. However, it is quite reasonable, because in this case several approximations for the analytical results are not valid any more. When Γ is not very large, the term $\mathcal{L}_s = \Gamma D_{\sigma_-}$ does not dominate over H in Eq. (3). As $\bar{n}_a$ is also at the same scale with $\bar{n}_b$ in this case, now neglecting the back action on mode a is not a good approximation. When mode b is being cooled, mode a is being heated unavoidably, thus lowering the effect of cooling. The analytical results which neglect the back action thus exaggerate the cooling effect. This trend is shown clearly from the figure. But the analytical conclusions are still valid qualitatively. For instance, if we fix Γ, as $\bar{n}_a$ is larger, the cooling effect also will be larger. And if we fix $\bar{n}_a$, there exists an $\bar{n}_a$-dependent value of Γ where the cooling effect is maximum.

V. DISCUSSION AND CONCLUSION

From the above derivation and calculation, it is clear that the higher frequency mechanical mode will be significantly cooled by heating the lower frequency mechanical mode. In fact, this trend can be seen directly from the Eq. (8), where $\mathcal{L}_1$ acts as the cooling term. As the electron spin is much more likely to be in the spin state $|0\rangle$ due to the continuous initialization, the effect of σ_+ should be much larger than that of σ_-. So $D_{b\sigma_+}$ is the dominant operator for evolution, and the mode b will be cooled. It can be understood that mode a facilitates the energy transfer between mode b and the spin. Quantized energy flows from the vibration mode to the NV center. Soon after that the excitation in the NV center electron spin decays into the environment through light. As this process is repeated, the heat of the mechanical mode b is gradually removed.

In conclusion, we studied the second-order magnetic gradient induced coupling between NV center and the mechanical modes. We proposed to drive one mechanical resonator mode with a thermal bath to cool the other mode of the resonator. We solved the motion of the system analytically under the weak coupling assumption. It is found that under a rotating wave approximation, the final thermal phonon number of the resonator approaches a minimum as the thermal bath temperature increases. The quantum regime cooling is feasible under the current experimental conditions. We numerically solved the equations, and found that the results fitted very well with the analytic results. The cooling by heating phenomena does not violate the laws of thermodynamics. This scheme can be understood as a thermal machine or a heat engine [46–48]. The mode a acts as an engine, and the NV center electron spin takes the role of a condenser. This work opens up the possibility of cooling the mechanical mode in solid systems by injecting the thermal phonon, which usually heats the system.

ACKNOWLEDGMENTS

Z.-q.Y. is supported by National Natural Science Foundation of China Grants No. 61435007 and No. 11574176. W.L.Y. is supported by National Natural Science Foundation of China Grants No. 11574353 and No. 11274351. P.H and J.D. are supported by the 973 Program (Grant No. 2013CB921800), the National Natural Science Foundation of China (Grant No. 11227901), and the CAS (Grant No. XDB01030400).

APPENDIX A: EXPERIMENTALLY REALIZED PARAMTERS

In this section we discuss the values of parameters ω_z, ω_a, ω_b, g_a, g_b, g_{ab}, γ_a, γ_b, and Γ that can be realized in experiments.

As in former experiments (e.g., Ref. [30] for a Si cantilever), the size of the resonator can be taken as around $3 \times 0.05 \times 0.05\ \mu$m. Considering that the density of diamond is around 1.5 times the density of silicon [49], and the fact that the effective mass of a solid and normally shaped oscillator doing simple oscillation is of the same order as its mass, we can estimate that $m_a = m_b = 5 \times 10^{-18}$ kg. The fundamental frequency of such a mechanical resonator is around 10 MHz [30]. Although the zero-field splitting of the NV center is around 2.88 GHz [50], after an external magnetic field is exerted, the separation between $|0\rangle$ and $|-1\rangle$ states can be reduced to the order of tens of MHz. As a result, it is possible to fulfill the requirement $\omega_b - \omega_a = \omega_z$. Here we choose $\omega_a/2\pi = 10$ MHz, $\omega_b/2\pi = 30$ MHz for convenience. The quality factor of the resonator can reach up to $Q = 10^7$ [49]. Second-order magnetic gradient G_2 can realize several times of 10^{13} T m^{-2} in experiments [51]. By using finite element simulation, we got that the maximum

G_2 could be around $5 \times 10^{14}\ \mathrm{T\,m^{-2}}$, if the distance between the NV center and the magnetic particles is 50 nm.

If G_2 is set to be $5 \times 10^{14}\ \mathrm{T\,m^{-2}}$, we will have $g_a/2\pi = 3$ Hz, $g_b/2\pi = 1$ Hz, and $g_{ab}/2\pi = 1.73$ Hz. The decay rates of the mechanical resonator can be estimated by $\gamma_a = \gamma_b = \omega_a/Q = 2\pi \times 1$ Hz. We need to tune the decay rate of the NV center to be much larger than the mechanical decay rate to reach ground-state cooling; for instance, Γ can equal to $2\pi \times 120$ Hz.

APPENDIX B: DERIVATION OF THE REDUCED MASTER EQUATION

Here we provide a derivation of the reduced master equation, Eq. (5) in the main text. The reduced density matrix of mode b and mode s after mode a is eliminated is

$$\rho_{b,s} = \mathrm{tr}_a(\rho). \tag{B1}$$

We can adiabatically eliminate mode a to get the evolution equation for the reduced density matrix [43]

$$\begin{aligned}\dot{\rho}_{b,s}(t) &= -i[H_0, \rho_{b,s}(t)] + \mathcal{L}_b\rho_{b,s}(t) + \mathcal{L}_s\rho_{b,s}(t) \\ &\quad + \mathrm{tr}_a\mathcal{L}_{\mathrm{int}}\int_0^\infty dt' e^{\mathcal{L}_{\mathrm{free}}t'}\mathcal{L}_{\mathrm{int}}\rho_{b,s}(t-t')\otimes\rho_a \\ &= -i[H_0, \rho_{b,s}(t)] + \mathcal{L}_b\rho_{b,s}(t) + \mathcal{L}_s\rho_{b,s}(t) \\ &\quad - \mathrm{tr}_a\left[H_1, \int_0^\infty dt' e^{\mathcal{L}_{\mathrm{free}}t'}[H_1, \rho_{b,s}(t-t')\otimes\rho_a]\right],\end{aligned} \tag{B2}$$

where we denote

$$\begin{aligned}\mathcal{L}_{\mathrm{int}} &= -i[H_1, \bullet], \\ \mathcal{L}_{\mathrm{free}} &= -i[H_0, \bullet] + \mathcal{L}_a + \mathcal{L}_b + \mathcal{L}_s.\end{aligned} \tag{B3}$$

We expand g_a, g_b and g_{ab} to the second order and can get

$$\begin{aligned}\dot{\rho}_{b,s}(t) = &-i[H_0, \rho_{b,s}(t)] + \mathcal{L}_b\rho_{b,s}(t) + \mathcal{L}_s\rho_{b,s}(t) \\ &- \mathrm{tr}_a\left[H_1, \int_0^\infty dt' [e^{\mathcal{L}_{\mathrm{free}}^\dagger t'}(H_1), \rho_{b,s}(t)\otimes\rho_a]\right].\end{aligned} \tag{B4}$$

Once we expand the commutation relations in Eq. (B4), we can directly calculate it term by term:

$$\begin{aligned}\dot{\rho}_{b,s}(t) = &-i[H_0, \rho_{b,s}(t)] + \mathcal{L}_b\rho_{b,s}(t) + \mathcal{L}_s\rho_{b,s}(t) \\ &- \mathrm{tr}_a\left\{\int_0^\infty dt' [H_1 e^{\mathcal{L}_{\mathrm{free}}^\dagger t'}(H_1)\rho_{b,s}(t)\otimes\rho_a \right. \\ &- H_1\rho_{b,s}(t)\otimes\rho_a e^{\mathcal{L}_{\mathrm{free}}^\dagger t'}(H_1) \\ &- e^{\mathcal{L}_{\mathrm{free}}^\dagger t'}(H_1)\rho_{b,s}(t)\otimes\rho_a H_1 \\ &\left. + \rho_{b,s}(t)\otimes\rho_a e^{\mathcal{L}_{\mathrm{free}}^\dagger t'}(H_1)H_1]\right\}.\end{aligned} \tag{B5}$$

What we need first is the term $e^{\mathcal{L}_{\mathrm{free}}^\dagger t'}(H_1)$. It is easy to get from direct calculation:

$$\begin{aligned}\mathcal{L}_{\mathrm{free}}^\dagger(a) &= (1+\bar{n}_a)\gamma_a D_a^\dagger(a) + \bar{n}_a\gamma_a D_{a^\dagger}^\dagger(a) \\ &= (1+\bar{n}_a)\gamma_a(2a^\dagger a^2 - a^\dagger a^2 - aa^\dagger a) \\ &\quad + \bar{n}_a\gamma_a(2a^2a^\dagger - aa^\dagger a - a^2a^\dagger) \\ &= -\gamma_a a.\end{aligned} \tag{B6}$$

Similarly, $\mathcal{L}_{\mathrm{free}}^\dagger(a^\dagger) = -\gamma_a a^\dagger$. From these we have $e^{\mathcal{L}_{\mathrm{free}}^\dagger t'}a = e^{-\gamma_a t'}a$, $e^{\mathcal{L}_{\mathrm{free}}^\dagger t'}a^\dagger = e^{-\gamma_a t'}a^\dagger$.

The following results are obtained using exactly the same method:

$$\begin{aligned}&e^{\mathcal{L}_{\mathrm{free}}^\dagger t'}\delta = e^{-2\gamma_a t'}\delta, \quad e^{\mathcal{L}_{\mathrm{free}}^\dagger t'}b = e^{-(\gamma_b + i\omega_z)t'}b, \\ &e^{\mathcal{L}_{\mathrm{free}}^\dagger t'}b^\dagger = e^{-(\gamma_b - i\omega_z)t'}b, \quad e^{\mathcal{L}_{\mathrm{free}}^\dagger t'}\sigma_+ = e^{(i\omega_z - \Gamma)t'}\sigma_+, \\ &e^{\mathcal{L}_{\mathrm{free}}^\dagger t'}\sigma_- = e^{(-i\omega_z - \Gamma)t'}\sigma_-.\end{aligned} \tag{B7}$$

$e^{\mathcal{L}_{\mathrm{free}}^\dagger t'}(H_1)$ will then be calculated with the results above in mind:

$$\begin{aligned}e^{\mathcal{L}_{\mathrm{free}}^\dagger t'}(H_1) &= g_a[(e^{\mathcal{L}_{\mathrm{free}}^\dagger t'}\delta)(e^{\mathcal{L}_{\mathrm{free}}^\dagger t'}\sigma_+) + (e^{\mathcal{L}_{\mathrm{free}}^\dagger t'}\delta)(e^{\mathcal{L}_{\mathrm{free}}^\dagger t'}\sigma_-)] \\ &\quad + g_{ab}[(e^{\mathcal{L}_{\mathrm{free}}^\dagger t'}a^\dagger)(e^{\mathcal{L}_{\mathrm{free}}^\dagger t'}b)(e^{\mathcal{L}_{\mathrm{free}}^\dagger t'}\sigma_+) \\ &\quad + (e^{\mathcal{L}_{\mathrm{free}}^\dagger t'}a)(e^{\mathcal{L}_{\mathrm{free}}^\dagger t'}b^\dagger)(e^{\mathcal{L}_{\mathrm{free}}^\dagger t'}\sigma_-)] \\ &= g_a\delta e^{-(2\gamma_a+\Gamma)t'}(\sigma_+ e^{i\omega_z t'} + \sigma_- e^{-i\omega_z t'}) \\ &\quad + g_{ab}e^{-(\gamma_a+\gamma_b+\Gamma)t'}(a^\dagger b\sigma_+ + ab^\dagger\sigma_-).\end{aligned} \tag{B8}$$

It deserves notice that here we only keep the slow-time-varying term, so we neglect $a^{\dagger 2}$ and a^2 above. Now we come back to Eq. (B5), which can be simplified term by term. As tr_a means taking the average on a, the trace of odd multiples of a and $a^\dagger$ equals to zero. Terms containing $i\omega_z$ are neglected here because their effect is just changing the energy zero point:

$$\begin{aligned}&\mathrm{tr}_a\left[\int_0^\infty dt' H_1 e^{\mathcal{L}_{\mathrm{free}}^\dagger t'}(H_1)\rho_{b,s}(t)\otimes\rho_a\right] \\ &= g_a^2(\bar{n}_a^2 + \bar{n}_a)\frac{2\gamma_a+\Gamma}{\omega_z^2 + (2\gamma_a+\Gamma)^2}(\sigma_+\sigma_- + \sigma_-\sigma_+)\rho_{b,s}(t) \\ &\quad + \frac{g_{ab}^2}{\gamma_a+\gamma_b+\Gamma}[(\bar{n}_a+1)b^\dagger\sigma_- b\sigma_+ + \bar{n}_a b\sigma_+ b^\dagger\sigma_-]\rho_{b,s}(t),\end{aligned} \tag{B9}$$

$$\begin{aligned}\mathrm{tr}_a\left[\int_0^\infty dt' H_1\rho_{b,s}(t)\otimes\rho_a e^{\mathcal{L}_{\mathrm{free}}^\dagger t'}(H_1)\right] &= g_a^2(\bar{n}_a^2 + \bar{n}_a)\frac{2\gamma_a+\Gamma}{\omega_z^2 + (2\gamma_a+\Gamma)^2}[\sigma_+\rho_{b,s}(t)\sigma_- + \sigma_-\rho_{b,s}(t)\sigma_+] \\ &\quad + \frac{g_{ab}^2}{\gamma_a+\gamma_b+\Gamma}[(\bar{n}_a+1)b\sigma_+\rho_{b,s}(t)b^\dagger\sigma_- + \bar{n}_a b^\dagger\sigma_-\rho_{b,s}(t)b\sigma_+],\end{aligned} \tag{B10}$$

$$\mathrm{tr}_a\left[\int_0^\infty dt' e^{\mathcal{L}_{\mathrm{free}}^\dagger t'}(H_1)\rho_{b,s}(t)\otimes\rho_a H_1\right] = g_a^2(\bar{n}_a^2+\bar{n}_a)\frac{2\gamma_a+\Gamma}{\omega_z^2+(2\gamma_a+\Gamma)^2}[\sigma_+\rho_{b,s}(t)\sigma_- + \sigma_-\rho_{b,s}(t)\sigma_+]$$
$$+\frac{g_{ab}^2}{\gamma_a+\gamma_b+\Gamma}[(\bar{n}_a+1)b\sigma_+\rho_{b,s}(t)b^\dagger\sigma_- + \bar{n}_a b^\dagger\sigma_-\rho_{b,s}(t)b\sigma_+], \quad \text{(B11)}$$

$$\mathrm{tr}_a\left[\int_0^\infty dt' \rho_{b,s}(t)\otimes\rho_a e^{\mathcal{L}_{\mathrm{free}}^\dagger t'}(H_1)H_1\right] = g_a^2(\bar{n}_a^2+\bar{n}_a)\frac{2\gamma_a+\Gamma}{\omega_z^2+(2\gamma_a+\Gamma)^2}\rho_{b,s}(t)(\sigma_+\sigma_- + \sigma_-\sigma_+)$$
$$+\frac{g_{ab}^2}{\gamma_a+\gamma_b+\Gamma}\rho_{b,s}(t)[(\bar{n}_a+1)b^\dagger\sigma_- b\sigma_+ + \bar{n}_a b\sigma_+ b^\dagger\sigma_-]. \quad \text{(B12)}$$

After we insert Eqs. (B9)–(B12) into Eq. (B5), we will get Eq. (5) in the main text.

APPENDIX C: DERIVATION OF THE ADJOINT EQUATIONS FOR THE NUMBER OPERATORS

In this part, the equations of motion for the number operators $\hat{n}_b$ and $\hat{n}_s$, Eq. (9) in the main text, is derived. The adjoint equations for Eq. (9) in the main text are

$$\frac{d}{dt}\hat{n}_s = (\mathcal{L}_1^\dagger + \mathcal{L}_s'^\dagger)\hat{n}_s = \frac{g_{ab}^2}{\gamma_a+\gamma_b+\Gamma}[(1+\bar{n}_a)D_{b\sigma_+}^\dagger + \bar{n}_a D_{b^\dagger\sigma_-}^\dagger]\hat{n}_s + [(1+n_s')\Gamma D_{\sigma_-}^\dagger + n_s'\Gamma D_{\sigma_+}^\dagger]\hat{n}_s,$$
$$\frac{d}{dt}\hat{n}_b = (\mathcal{L}_1^\dagger + \mathcal{L}_b^\dagger)\hat{n}_b = \frac{g_{ab}^2}{\gamma_a+\gamma_b+\Gamma}[(1+\bar{n}_a)D_{b\sigma_+}^\dagger + \bar{n}_a D_{b^\dagger\sigma_-}^\dagger]\hat{n}_b + [(1+\bar{n}_b)\gamma_b D_b^\dagger + \bar{n}_b\gamma_b D_{b^\dagger}^\dagger]\hat{n}_b. \quad \text{(C1)}$$

From simple calculations, we have

$$D_{b\sigma_+}^\dagger(\hat{n}_s) = 2(1-\hat{n}_s)\hat{n}_b, \quad D_{b^\dagger\sigma_-}^\dagger(\hat{n}_s) = -2\hat{n}_s(1+\hat{n}_b),$$
$$D_{\sigma_+}^\dagger(\hat{n}_s) = 2(1-\hat{n}_s), \quad D_{\sigma_-}^\dagger(\hat{n}_s) = -2\hat{n}_s,$$
$$D_{b\sigma_+}^\dagger(\hat{n}_b) = -2(1-\hat{n}_s)\hat{n}_b, \quad D_{b^\dagger\sigma_-}^\dagger(\hat{n}_b) = 2\hat{n}_s(1+\hat{n}_b),$$
$$D_b^\dagger(\hat{n}_b) = -2\hat{n}_b, \quad D_{b^\dagger}^\dagger(\hat{n}_b) = 2(1+\hat{n}_b). \quad \text{(C2)}$$

After Eq. (C2) is inserted into Eq. (C1), it will be simplified to Eq. (9) in the main text.

APPENDIX D: DETAIL OF THE NUMERICAL SIMULATION

In this section, we discuss in detail the numerical simulation. For Fig. 4 in the main text, we control the accuracy so that all numbers are accurate until the order of 0.001. The evolution time is $t = 3$, after which the state is at the stationary state up to the accuracy. As discussed in Appendix A, we can choose the frequency parameters as $g_{ab}/2\pi = \sqrt{3}$ Hz, $g_a/2\pi = 1$ Hz, $g_{ab}/2\pi = 3$ Hz, $\gamma_a/2\pi = \gamma_b/2\pi = 1$ Hz. As we want to cover a wide range of results, four values $\Gamma/2\pi$ are chosen: 2, 15, 50, and 120. Small values for the phonon numbers $\bar{n}_a$ and $\bar{n}_b$ should be chosen due to the calculation cost.

Here we always choose $\bar{n}_b = 1$ as the initial condition. As to $\bar{n}_a$, we choose $\bar{n}_a = 1,2,3,4$. The dimensions of the matrices in the Hilbert space are chosen to balance the accuracy and the cost of calculation resource. For the Hilbert space where the initial phonon number equals 1, the dimension is chosen as 15×15. For the Hilbert space where the initial phonon number equals 2, the dimension is chosen as 27×27. For the Hilbert space where the initial phonon number equals 3, the dimension is chosen as 40×40. For the Hilbert space where the initial phonon number equals 4, the dimension is chosen as 60×60. Obviously, the dimension of the Hilbert space for mode s is always 2×2. The step length for the Runge-Kutta method is chosen to be 0.01/50.

Figure 4 in the main text shows the results of only the $\omega_z = 500$ case, even if for the example in Appendix A, $\omega_z/2\pi$ should be chosen as $\omega_z/2\pi = 2\times 10^7$. In fact, different $\omega_z/2\pi$ will not influence the result of cooling; e.g., $\omega_z = 250$, 500, 750 all give out same final phonon number for mode b. So we

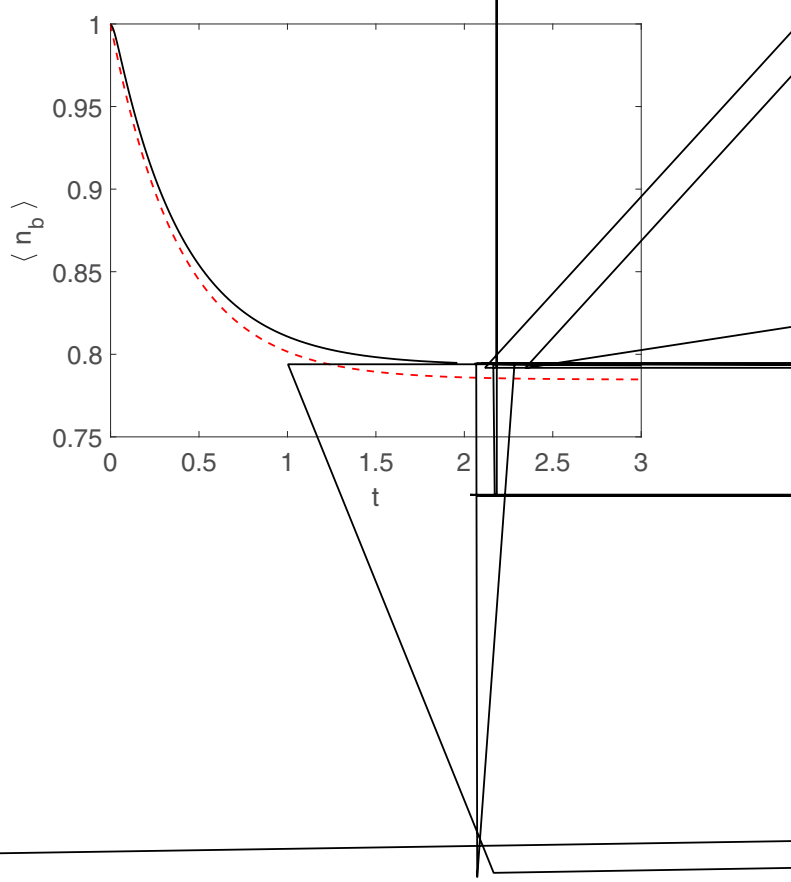

are safe to use smaller ω_z here, considering the stability of the simulation. This deduction also agrees with the analytical result because Eq. (10) in the main text does not contain ω_z as long as ω_z is large enough for $n_s^{'} \approx 0$.

The time evolution of one set of parameters from numerical simulation is shown in Fig. 5. The phonon occupation number $\langle \hat{n}_b \rangle$ gradually goes down as the system evolves towards the stationary state. The cooling effect indeed happens. Also shown in the figure is the time evolution starting from the analytical result, Eq. (9). The two lines are similar, with the cooling effect of the analytical one a little bit more obvious, which also supports our findings.

[1] M. Aspelmeyer, T. J. Kippenberg, and F. Marquardt, Rev. Mod. Phys. **86**, 1391 (2014).
[2] C. A. Regal and K. W. Lehnert, J. Conf. Ser. **264**, 012025 (2011).
[3] S. Barzanjeh, M. Abdi, G. J. Milburn, P. Tombesi, and D. Vitali, Phys. Rev. Lett. **109**, 130503 (2012).
[4] Y.-D. Wang and A. A. Clerk, Phys. Rev. Lett. **108**, 153603 (2012).
[5] L. Tian, Phys. Rev. Lett. **108**, 153604 (2012).
[6] S. Rips and M. J. Hartmann, Phys. Rev. Lett. **110**, 120503 (2013).
[7] Z.-q. Yin and Y.-J. Han, Phys. Rev. A **79**, 024301 (2009).
[8] Z.-q. Yin, W. L. Yang, L. Sun, and L. M. Duan, Phys. Rev. A **91**, 012333 (2015).
[9] S. Barzanjeh, S. Guha, C. Weedbrook, D. Vitali, J. H. Shapiro, and S. Pirandola, Phys. Rev. Lett. **114**, 080503 (2015).
[10] R. Penrose, Gen. Relativ. Gravit. **28**, 581 (1996).
[11] A. D. O'Connell, M. Hofheinz, M. Ansmann, R. C. Bialczak, M. Lenander, E. Lucero, M. Neeley, D. Sank, H. Wang, and M. Weides, Nature (London) **464**, 697 (2010).
[12] J. Teufel, T. Donner, D. Li, J. Harlow, M. Allman, K. Cicak, A. Sirois, J. D. Whittaker, K. Lehnert, and R. W. Simmonds, Nature (London) **475**, 359 (2011).
[13] M. Poot and H. S. J. van der Zant, Phys. Rep. **511**, 273 (2012).
[14] I. Pikovski, M. R. Vanner, M. Aspelmeyer, M. Kim, and Č. Brukner, Nat. Phys. **8**, 393 (2012).
[15] S. Nimmrichter and K. Hornberger, Phys. Rev. Lett. **110**, 160403 (2013).
[16] A. Bassi, K. Lochan, S. Satin, T. P. Singh, and H. Ulbricht, Rev. Mod. Phys. **85**, 471 (2013).
[17] O. Romero-Isart, A. C. Pflanzer, F. Blaser, R. Kaltenbaek, N. Kiesel, M. Aspelmeyer, and J. I. Cirac, Phys. Rev. Lett. **107**, 020405 (2011).
[18] Z.-q. Yin, T. Li, X. Zhang, and L. M. Duan, Phys. Rev. A **88**, 033614 (2013).
[19] T. Li and Z. Yin, Sci. Bull. **61**, 163 (2016).
[20] S. Barzanjeh and D. Vitali, Phys. Rev. A **93**, 033846 (2016).
[21] C. M. Caves, Phys. Rev. D **23**, 1693 (1981).
[22] A. A. Geraci, S. B. Papp, and J. Kitching, Phys. Rev. Lett. **105**, 101101 (2010).
[23] Z.-q. Yin, T. Li, and M. Feng, Phys. Rev. A **83**, 013816 (2011).
[24] A. Arvanitaki and A. A. Geraci, Phys. Rev. Lett. **110**, 071105 (2013).
[25] P. Huang, P. Wang, J. Zhou, Z. Wang, C. Ju, Z. Wang, Y. Shen, C. Duan, and J. Du, Phys. Rev. Lett. **110**, 227202 (2013).
[26] N. Zhao and Z.-q. Yin, Phys. Rev. A **90**, 042118 (2014).
[27] I. Wilson-Rae, N. Nooshi, W. Zwerger, and T. J. Kippenberg, Phys. Rev. Lett. **99**, 093901 (2007).
[28] F. Marquardt, J. P. Chen, A. A. Clerk, and S. M. Girvin, Phys. Rev. Lett. **99**, 093902 (2007).
[29] L. Yong-Chun, H. Yu-Wen, W. C. We, and X. Yun-Feng, Chin. Phys. B **22**, 114213 (2013).
[30] P. Rabl, P. Cappellaro, M. V. G. Dutt, L. Jiang, J. R. Maze, and M. D. Lukin, Phys. Rev. B **79**, 041302(R) (2009).
[31] E. R. MacQuarrie, M. Otten, S. K. Gray, and G. D. Fuchs, arXiv:1605.07131.
[32] P.-B. Li, Z.-L. Xiang, P. Rabl, and F. Nori, Phys. Rev. Lett. **117**, 015502 (2016).
[33] A. Mari and J. Eisert, Phys. Rev. Lett. **108**, 120602 (2012).
[34] Z. Yin, Phys. Rev. A **80**, 033821 (2009).
[35] L.-g. Zhou, L. F. Wei, M. Gao, and X.-b. Wang, Phys. Rev. A **81**, 042323 (2010).
[36] Z. Y. Xu, Y. M. Hu, W. L. Yang, M. Feng, and J. F. Du, Phys. Rev. A **80**, 022335 (2009).
[37] Q. Chen, Z. Xu, and M. Feng, Phys. Rev. A **82**, 014302 (2010).
[38] O. Arcizet, V. Jacques, A. Siria, P. Poncharal, P. Vincent, and S. Seidelin, Nat. Phys. **7**, 879 (2011).
[39] S. Kolkowitz, A. C. Jayich, Q. P. Unterreithmeier, S. D. Bennett, P. Rabl, J. G. Harris, and M. D. Lukin, Science **335**, 1603 (2012).
[40] Z. Yin, N. Zhao, and T. Li, Sci. China Phys. Mech. Astron. **58**, 1 (2015).
[41] J. Cai, B. Naydenov, R. Pfeiffer, L. P. McGuinness, K. D. Jahnke, F. Jelezko, M. B. Plenio, and A. Retzker, New J. Phys. **14**, 113023 (2012).
[42] H. Breuer and F. Petruccione, *The Theory of Open Quantum Systems* (Oxford University Press, Oxford, UK, 2002).
[43] C. Gardiner and P. Zoller, *Quantum Noise: A Handbook of Markovian and Non-Markovian Quantum Stochastic Methods with Applications to Quantum Optics* (Springer Science and Business Media, Berlin, 2004), p. 56.
[44] Z.-q. Yin, F.-l. Li, and P. Peng, Phys. Rev. A **76**, 062311 (2007).
[45] C.-J. Yang, J.-H. An, W. Yang, and Y. Li, Phys. Rev. A **92**, 062311 (2015).
[46] K. Zhang, F. Bariani, and P. Meystre, Phys. Rev. Lett. **112**, 150602 (2014).
[47] A. Mari, A. Farace, and V. Giovannetti, J. Phys. B **48**, 175501 (2015).
[48] M. T. Mitchison, M. Huber, J. Prior, M. P. Woods, and M. B. Plenio, Quantum Sci. Technol. **1**, 015001 (2016).
[49] Y. Tao, J. Boss, B. Moores, and C. Degen, Nat. Commun. **5**, 3638 (2014).
[50] J. Wrachtrup and F. Jelezko, J. Phys.: Condens. Matter **18**, S807 (2006).
[51] H. Mamin, M. Poggio, C. Degen, and D. Rugar, Nat. Nanotechnol. **2**, 301 (2007).